Fluids in porous media: The case of neutral walls

Giuseppe Pellicane,[1,2] Richard L. C. Vink,[3] Bruno Russo,[4] and Paolo V. Giaquinta[5]

[1]*School of Chemistry and Physics, University of Kwazulu-Natal, Private Bag X01, Scottsville 3209, Pietermaritzburg, South Africa*

[2]*National Institute for Theoretical Physics (NITheP), KZN node, Pietermaritzburg, South Africa*

[3]*Institute of Theoretical Physics, Georg-August-Universität, Friedrich-Hund-Platz 1, D-37077 Göttingen, Germany*

[4]*Techimp Corporate Headquarter, Via Toscana, 11/c, 40069 Zola Predosa (BO), Italy*

[5]*Dipartimento di Fisica e di Scienze della Terra, Università degli Studi di Messina, Viale F. Stagno d'Alcontres 31, 98166 Messina, Italy*

(Received 9 August 2013; published 18 October 2013)

The bulk phase behavior of a fluid is typically altered when the fluid is brought into confinement by the walls of a random porous medium. Inside the porous medium, phase-transition points are shifted, or may disappear altogether. A crucial determinant is how the walls interact with the fluid particles. In this work, we consider the situation whereby the walls are neutral with respect to the liquid and vapor phases. In order to realize the condition of strict neutrality, we use a symmetric binary mixture inside a porous medium that interacts identically with mixture species. Monte Carlo simulations are then used to obtain the phase behavior. Our main finding is that, in the presence of the porous medium, a liquid-vapor critical point still exists. At the critical point, the distribution of the order parameter remains scale invariant, but self-averaging is violated. These findings provide further evidence that random confinement by neutral walls induces critical behavior of the random Ising model (i.e., Ising models with dilution type disorder, where the disorder couples to the energy).

DOI: 10.1103/PhysRevE.88.042131 PACS number(s): 05.70.Jk, 02.70.−c

I. INTRODUCTION

The confinement of a fluid to the voids of a porous material generally influences the critical behavior of the fluid. For example, lutidine-water mixtures in Vycor [1], or ^{4}He [2], nitrogen [3], and carbon dioxide [4] in silica aerogel yield critical exponents of their associated liquid-vapor transitions that differ profoundly from bulk values (the bulk exponents typically being those of the three-dimensional Ising model). One line of thought is that the random pore structure induces quenched spatial fluctuations in the chemical potential [5]. This conjecture, originally put forward by de Gennes [6], implies that the critical behavior of the fluid inside the pores should be that of the random-field Ising model (RFIM) [7–9]. Recent simulations of fluids inside porous media have indeed uncovered critical behavior characteristic of the RFIM [10–13]. In order for RFIM universality to arise, it is crucial that the pore walls feature a preferred attraction to one of the fluid phases. This condition is typically fulfilled in experiments, as one of the phases, i.e., the liquid or the vapor, is frequently seen to wet the pore walls [1,3,4].

Nevertheless, for our fundamental understanding of fluid-phase behavior, the situation of "neutral" pore walls which do not preferentially attract is of interest also. A different universality class is then expected to come into play [14,15], namely the one of the random Ising model (RIM). The defining feature of the RIM is that the quenched randomness of the porous medium couples to the energy (as opposed to the order parameter in the RFIM). Typical lattice models that belong to the universality class of the RIM are the site-diluted Ising model [16,17], the bond-diluted Ising model [17,18], and the random-bond Ising model [19]. In $d = 3$ dimensions, the Harris criterion [20] implies that the RIM should still feature a liquid-vapor critical point, but with critical exponents different from those of the *bulk* Ising model (by "*bulk*" we mean in the absence of the porous medium). In a heuristic derivation of this criterion one assumes that, in the presence of quenched disorder, the critical temperature T_c varies between regions (of linear size ξ) in the sample. Hence, following the central limit theorem, there is a fluctuation $\Delta T \propto \xi^{-d/2}$ in the observed critical temperatures, where d is the spatial dimension. A prerequisite for the universality class to remain unchanged is that ΔT be smaller than the distance from the critical temperature $t = |T - T_c|$. Since $\xi \propto t^{-\nu}$ $(t \ll 1)$, with ν the (bulk) correlation length critical exponent, $d\nu > 2$ is implied; by using hyperscaling, $d\nu = 2 - \alpha$, this becomes equivalent to $\alpha < 0$, where α is the specific heat critical exponent. For the bulk Ising model in $d = 3$ dimensions α is positive, which implies that the universality class of the RIM should be different.

Note, however, that the differences between the universality classes of the bulk Ising model and the RIM are very small, and therefore challenging to detect numerically [18]. One problem is that the critical exponent ratios are very similar in both classes, which greatly complicates finite-size scaling, unless extremely accurate data is available. In fact, for the random-bond Ising model, such data have only recently been published [19]. Clearly, for the *off-lattice* fluid model considered presently, we cannot expect to reach the accuracy of that latter study (which is required if critical exponents are to be meaningfully measured). Fortunately, following Ref. [18], the difference in universality can also be probed *qualitatively* by considering the violations of self-averaging. It is this latter approach that will be adopted in this paper.

Regarding the case of a fluid confined to a neutral porous medium, the question of whether this system exhibits RIM universality was first addressed in the simulations of Ref. [15]. As expected for the RIM, these simulations revealed a critical point, located at an increased density as compared to the bulk. By carefully measuring the critical amplitude ratio of the susceptibility, these simulations also uncovered deviations from bulk Ising behavior, and toward that of the RIM. The aim of this work is to corroborate these findings, using a more sophisticated (grand-canonical) simulation scheme,

larger system sizes, as well as additional finite-size scaling methods. In particular, as mentioned above, we will address the question of self-averaging.

The outline of this paper is as follows. In Sec. II, we introduce the model for the fluid mixture and for the porous medium with neutral walls, and we describe the simulation method. The results are presented in Sec. III, and we end with a discussion in Sec. IV.

II. MODEL AND METHODS

A. Model: Fluid inside neutral porous medium

We consider the same model as in Ref. [15], which is a fluid confined to a neutral porous medium in $d = 3$ spatial dimensions. It belongs to the family of "quenched-annealed" mixtures [21,22], which are routinely used to model fluids inside pores [10,14,23–32]. The fluid is a nonadditive binary mixture of spheres, species A and B, of equal diameter σ. In what follows, σ will be our unit of length. The particles interact via hard-sphere pair potentials

$$u_{AA}(r) = u_{BB}(r) = \begin{cases} \infty, & r < \sigma, \\ 0 & \text{otherwise}, \end{cases}$$
$$u_{AB}(r) = \begin{cases} \infty, & r < (1+\Delta)\sigma, \\ 0 & \text{otherwise}, \end{cases} \tag{1}$$

with r the center-to-center distance between a pair of particles, and Δ the nonadditivity parameter. The porous medium is a fixed configuration of nonoverlapping spheres, species M, also of diameter σ. These spheres are distributed randomly at the start of the simulation, with density ρ_M, but remain immobile (quenched) thereafter. Only after the porous medium has been generated are the (mobile) fluid particles inserted. Note that Eq. (1) is symmetric under the exchange of particle labels $A \leftrightarrow B$. In order to retain this symmetry, the medium particles M interact symmetrically with the mobile fluid particles: $u_{AM}(r) = u_{BM}(r) \equiv u_{AA}(r)$. In this way, we ensure that the porous medium remains neutral, i.e., does not preferentially attract one of the fluid species. As a consequence, we do *not* expect the critical behavior of the RFIM for this system.

For $\Delta > 0$, the model of Eq. (1) exhibits a liquid-vapor type transition [33]. To analyze this transition, we introduce the overall fluid density $\rho = (N_A + N_B)/V$, and the composition (order parameter)

$$m = (N_A - N_B)/V, \tag{2}$$

where N_α is the number of particles of species α, and V the volume of the system. Provided $\rho > \rho_{\rm cr}$, two fluid phases are observed, I and II, characterized by a positive and negative composition, m_I and m_{II}, respectively (due to symmetry $m_I = -m_{II}$). Precisely for $\rho = \rho_{\rm cr}$, the system becomes critical, where $m_I = m_{II} = 0$. We emphasize that $\rho_{\rm cr}$ is not trivially known beforehand (its value depends on Δ and ρ_M). For $\rho < \rho_{\rm cr}$, the system exhibits only one phase. Of course, this behavior is analogous to that of the Ising model, if one identifies m in Eq. (2) with the magnetization per spin [34,35].

Our model is thus defined by the nonadditivity parameter Δ, and by the density of the porous medium ρ_M. In the following we set $\Delta = 0.2$, while for the porous medium $\rho_M = 0.1$ and 0.2 will be considered, as well as the bulk situation $\rho_M = 0$. These values were chosen to facilitate the comparison to previous studies [10,15,33].

B. Method: Grand-canonical Monte Carlo

Our simulations are performed in the grand-canonical (GC) ensemble, where the volume V is constant, while the particle numbers N_α can fluctuate freely, as governed by the fugacity z_α. Here, $\alpha \in \{A, B\}$ strictly refers to the mobile fluid, since the porous medium is quenched. Due to the symmetry of the model, it follows that $N_A = N_B$ at criticality, and so we set the particle fugacities equal: $z_A = z_B \equiv z$. The corresponding Boltzmann weight of a given particle configuration $w \propto z^{N_A+N_B} e^{-E/k_BT}$, with E the potential energy given by Eq. (1), T the temperature, and k_B the Boltzmann constant. Of course, for hard spheres, T does not affect static equilibrium properties, and thus is irrelevant. The sole control parameter in our simulations is therefore the fugacity z. In this work, we use standard single-particle Monte Carlo moves [36] to generate particle configurations that conform to the weight w. To enhance efficiency, histogram reweighting is used to extrapolate data obtained for one value of z to different (nearby) values [37]. The simulations are performed in a cubic box of edge L with periodic boundaries.

The principal output of the simulations is the (normalized) distribution

$$P(m) \equiv P(m|z, L, \rho_M), \qquad \int_{-\infty}^{\infty} P(m)dm = 1, \tag{3}$$

defined as the probability to observe the system in a state with composition m, with m given by Eq. (2). We emphasize that $P(m)$ depends on all the system parameters, in particular the fugacity z, and the system size L. Note also that, due to symmetry, $P(m) = P(-m)$, and that this symmetry holds irrespective of whether a porous medium is present.

To facilitate a finite-size scaling analysis (both for the bulk system, and inside the porous medium) four different system sizes were simulated. The smallest system has volume $(L/\sigma)^3 = 2500$, corresponding to $L/\sigma \approx 13.57$; the linear sizes L of the other systems increase in steps of 3.5σ, i.e., $L/\sigma \approx 17.07; 20.57; 24.07$ (in the figure legends, we report the system size rounded down to the nearest integer; our analysis uses the exact values, of course). For these system sizes, the total number of mobile particles ranged approximately between 1200 and 6000. The simulations were equilibrated for at least 10^5 GC cycles, and averages were obtained following production runs of 10^6–10^7 GC cycles (longer runs were performed for state points close to the critical point). A GC cycle consists of a number of attempted MC steps equal to the average total number of particles in the system.

For the fluid mixture inside the porous medium, $\rho_M > 0$, results were additionally averaged over $M = 100$ different configurations of the porous medium. The medium configurations were generated by equilibrating a system of hard spheres at fixed density ρ_M using canonical Monte Carlo moves for at least 10^6 cycles (here a cycle is defined as one attempted move per particle; as a canonical move we used random displacements of single particles). After equilibration, M configurations were collected and stored at intervals of

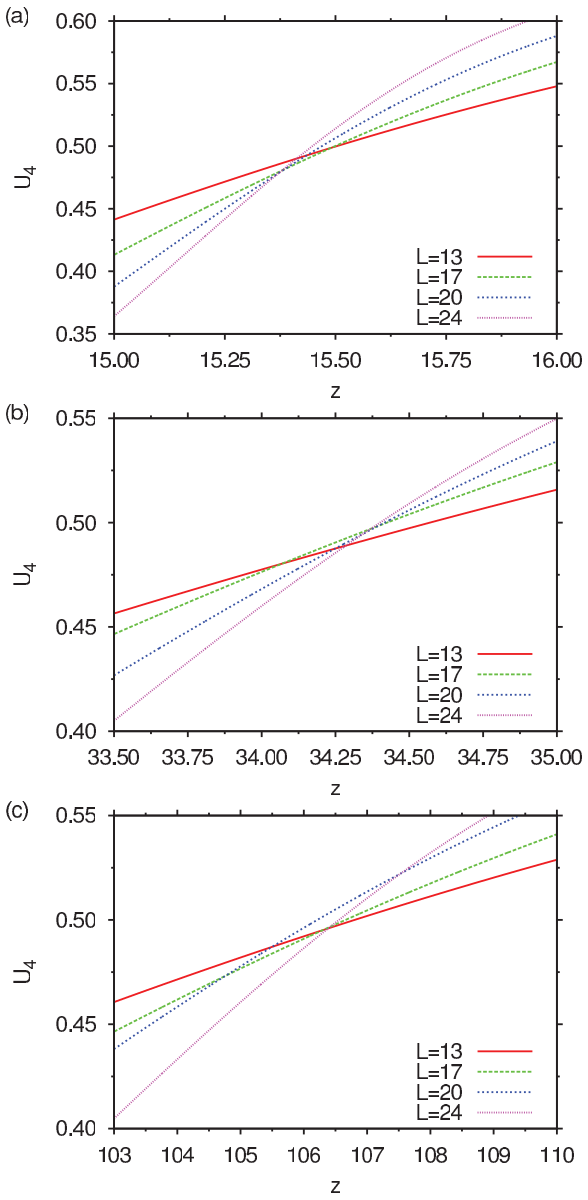

FIG. 1. (Color online) Binder cumulant U_4 as a function of the fugacity z for different system sizes L. The upper panel (a) shows the bulk result. Panels (b) and (c) show the result obtained in the presence of the porous medium, at medium densities $\rho_M = 0.1$ and 0.2, respectively. The intersection of the curves for different values of L yields the critical fugacity $z_{\rm cr}$ (Table I).

10^5 cycles. Then, the mobile AB particles of the fluid binary mixture were randomly inserted in the hollow cavities of the porous medium, and the distribution $P(m)$ of Eq. (3) was obtained in production runs lasting 10^6–10^7 GC cycles.

III. RESULTS

A. Locating the critical point

Our first aim is to locate the critical point of the transition. To this end, it is convenient to consider how the shape of the distribution $P(m)$ changes with the fugacity. In the bulk, we recover the behavior typical of a critical transition. At high fugacity, $P(m)$ is bimodal with two well-resolved peaks, indicating two-phase coexistence. At low fugacity, $P(m)$ is a single peak centered around $m = 0$. At intermediate fugacities, the system becomes critical, where $P(m)$ remains bimodal, but with overlapping peaks. The critical fugacity $z_{\rm cr}$ is obtained via the Binder cumulant

$$U_4 = 1 - \frac{\langle m^4 \rangle}{3\langle m^2 \rangle^2}, \quad \langle m^p \rangle = \int_{-\infty}^{\infty} m^p P(m) dm, \tag{4}$$

which becomes L independent at the critical point [38]. In Fig. 1(a), we plot U_4 as a function of z, for various system sizes L. In agreement with the existence of a critical point, we observe a regime of fugacities where the curves intersect. For each pair of system sizes, the fugacity at the cumulant intersection was determined, and subsequently averaged over all pairs. The latter serves as our estimate of the critical fugacity $z_{\rm cr}$ and is reported in Table I; the numbers in the brackets are the lowest and highest fugacities that were observed between all intersections, which reflects the uncertainty of our estimate.

At the critical point, not only the cumulant is scale invariant, but in fact the entire distribution $P(m)$ [38,39]

$$z = z_{\rm cr}: \quad P(m) \propto P^\star(a_m L^{\beta/\nu} m), \tag{5}$$

with β (ν) the critical exponent of the order parameter (correlation length), $P^\star(x)$ a scaling function that does not depend on system size, and constant a_m. The critical exponents, as well as $P^\star(x)$, are characteristic of the universality class. We provide numerical estimates of the critical exponents for bulk Ising and RIM universality in Table II. In Fig. 2(a), we plot $P(m)$ obtained at criticality, but with the horizontal axis scaled to conform to Eq. (5), using bulk Ising exponents. We observe that the data for different L collapse, consistent with a bulk Ising critical point. However, one should take these observations with some caution, as the critical properties of the RIM are very similar. Note that, in Fig. 2, only the exponent ratio β/ν enters as a parameter which is, in fact, essentially identical for both universality classes (and the same holds for γ/ν, with γ the susceptibility critical exponent). Therefore, while the data clearly show the presence of a critical point, they do not unambiguously identify the universality class

TABLE I. Critical-point properties of the fluid mixture confined to a neutral porous medium of density ρ_M as obtained in this work. Listed are the critical fugacity $z_{\rm cr}$, and the critical density $\rho_{\rm cr}$, both with uncertainty.

ρ_M	$z_{\rm cr}$	$\rho_{\rm cr}$
0	15.41 (15.37; 15.49)	0.4302(5)
0.1	34.3 (34.1; 34.4)	0.4032(5)
0.2	106.1 (104.8; 107.5)	0.380(1)

TABLE II. Selected critical properties of the bulk Ising model, and of the random Ising model (RIM) taken from various references [17,41]; the uncertainty reflects the typical range of reported values. The spatial dimension $d = 3$.

	β/ν	γ/ν	ν
Ising	0.517(3)	1.966(3)	0.6304(13)
RIM	0.519(3)	1.963(5)	0.6837(53)

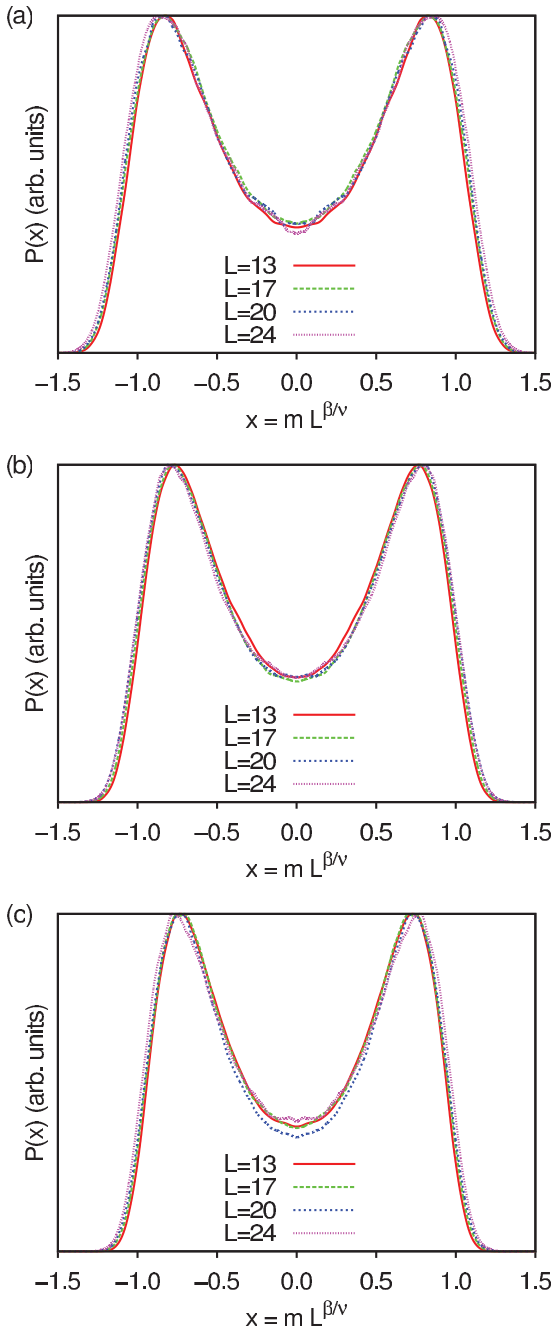

FIG. 2. (Color online) Distribution $P(m)$ obtained at the critical fugacity $z = z_{cr}$ for various system sizes L and scaled conform Eq. (5). The upper panel (a) shows the bulk result ($\rho_M = 0$) using bulk Ising critical exponents. Panels (b) and (c) show the result obtained in the presence of the porous medium, at medium density $\rho_M = 0.1$ and 0.2, respectively, where RIM critical exponents were used. Note that, in all panels, the distributions were explicitly symmetrized "by hand" after the simulation was completed.

(although, for the bulk case, there is no reason to doubt Ising universality [33,35,40].

In the presence of the porous medium, the behavior of $P(m)$ is similar, and a critical point can still be identified. The only complication is that results must be meaningfully averaged over the $M = 100$ medium configurations. In contrast to the RFIM [8,11], we observed that the peak positions in $P(m)$ did not fluctuate much between different configurations of the porous medium. For this reason, the probability distributions were simply averaged to yield the disorder averaged distribution

$$[P(m)] \equiv \frac{1}{M} \sum_{i=1}^{M} P^{(i)}(m), \tag{6}$$

where i labels the medium configurations. The cumulant analysis of $[P(m)]$ is presented in Fig. 1, panels (b) and (c), for $\rho_M = 0.1$ and 0.2, respectively. We again observe that curves for different values of L intersect, enabling rather accurate estimates of z_{cr} (Table I). The scaling of $[P(m)]$ at criticality is confirmed in the corresponding panels of Fig. 2, where the critical exponents of the RIM were used. Again, we emphasize that this analysis accurately locates the critical point, but it does not warrant conclusions concerning the universality class.

We also estimated the critical density ρ_{cr}. To this end, we monitored how the density ρ_L varied with the system size L, with ρ_L obtained in the finite system at the critical fugacity $z = z_{cr}$ of Table I. The latter were subsequently extrapolated to the thermodynamic limit using $\rho_{cr} - \rho_L \propto 1/L$. We thus ignore any singular behavior in ρ_{cr}, which is justified for our purposes since the shift $\rho_{cr} - \rho_L$ is typically small. The resulting estimates of ρ_{cr} are reported in Table I. The listed uncertainties reflect the scatter due to the uncertainty in z_{cr}. Our estimate of the bulk critical density compares well to $\rho_{cr} = 0.4299$ obtained in semigrand canonical simulations [33]. Note that, while z_{cr} increases with ρ_M, ρ_{cr} decreases. The increase of z_{cr} conforms to a "kelvin-like" behavior, i.e., a suppression of the transition temperature upon increasing confinement. The decrease of ρ_{cr} most likely reflects the fact that an increasing fraction of space is occupied by the quenched particles.

B. Correlation length critical exponent

We now attempt to measure the critical exponent ν of the correlation length, using the finite-size scaling approach of Ref. [42]. To this end, we select two of our data sets, corresponding to different system sizes, L_1 and L_2. We then vary the fugacity, and plot the cumulant $y = U_4(L_2)$ of the system with size L_2 versus $x = U_4(L_1)$ of the system with size L_1 (the curve is thus parametrized by the fugacity z). An example is provided in Fig. 3. The critical point corresponds to the fixed-point condition $U_4(L_1) = U_4(L_2)$, i.e., where the curve $y(x)$ intersects the line $y = x$ (indicated by the dot). The correlation length critical exponent is determined by the slope $s = y'(x)$ evaluated at the fixed point

$$\nu = \ln b / \ln s, \quad b = L_2/L_1. \tag{7}$$

Since $y(x)$ is essentially linear around the fixed point, the slope s can be determined rather accurately.

In Fig. 4, we plot the resulting estimates of ν versus ρ_M. Since, for each value of ρ_M, we have data for four different system sizes, a total of six measurements could be made each time. The dots in Fig. 4 show the average of these measurements, while the error bars reflect the root-mean-square deviation. Clearly, the errors are rather large. However, we do observe that ν inside the porous medium exceeds the

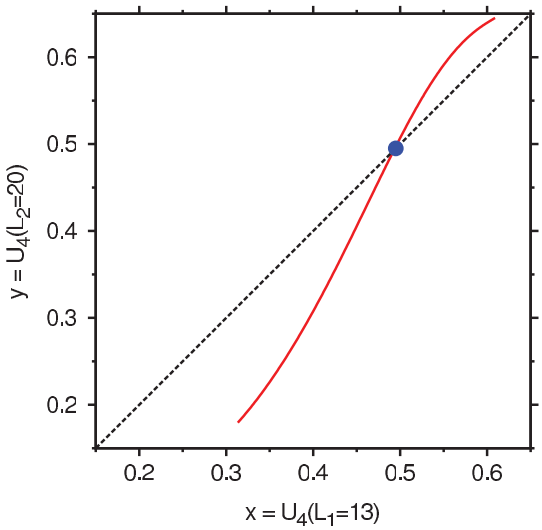

FIG. 3. (Color online) Demonstration of the method of Ref. [42] to determine the correlation length critical exponent ν (data refer to the bulk system). The solid curve shows the cumulant of the system with size L_2, versus the cumulant of the system with size L_1. The intersection of this curve with the line $y = x$ (dashed) marks the critical point (dot). The slope s of the solid curve at the critical point is related to ν via Eq. (7).

bulk value, a trend which is at least qualitatively consistent with RIM universality.

C. Distribution of pseudotransition points

We now consider the distribution of pseudotransition points; the latter are frequently encountered in systems containing quenched disorder, and their analysis has attracted much attention [43–47]. To be more specific, in a finite system of size L, the fugacity $z_{L,i}$ where the system becomes pseudocritical fluctuates between the $i = 1, \ldots, M$ realizations of the porous medium (the term pseudocritical is used because a finite system never becomes truly critical). The pseudocritical fugacity $z_{L,i}$ may be defined as the fugacity

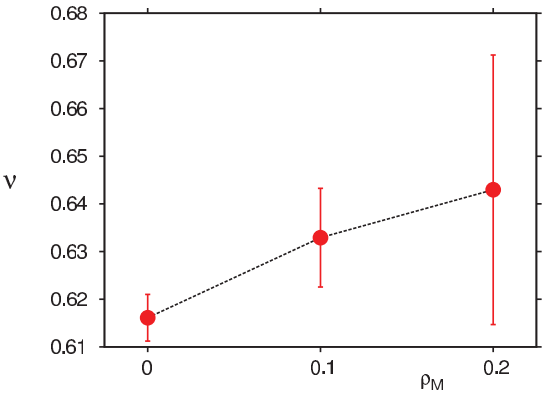

FIG. 4. (Color online) Correlation length critical exponent ν plotted versus the density of the porous medium ρ_M, as obtained using the method of Ref. [42]. The data reveal that ν inside the porous medium exceeds the bulk value, in qualitative agreement with RIM universality.

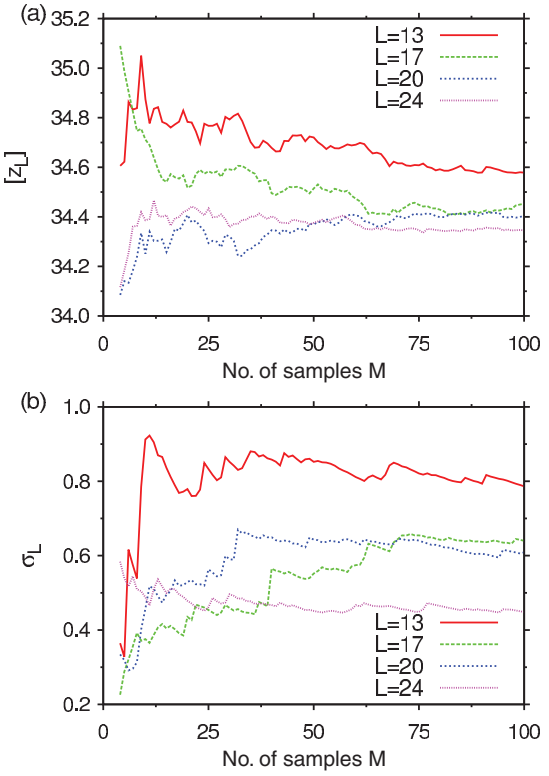

FIG. 5. (Color online) (a) "Running average" of the disorder averaged pseudotransition fugacity $[z_L]$ versus the number of quenched disorder samples M, for various system sizes L. (b) The same, but for the fluctuation σ_L. All data refer to porous medium density $\rho_M = 0.1$.

where the susceptibility

$$\chi_{L,i} = V(\langle m^2 \rangle - \langle |m| \rangle^2), \tag{8}$$

reaches its maximum, as measured in the ith realization of the porous medium, with m given by Eq. (2).

The key question is how the disorder fluctuation

$$\sigma_L^2 = [z_L^2] - [z_L]^2, \quad [X_L^p] = \frac{1}{M} \sum_{i=1}^{M} X_{L,i}^p, \tag{9}$$

decays with the system size L. In general, one expects a power-law decay: $\sigma_L \propto 1/L^k$, with $k > 0$. According to the Brout argument $k = d/2$, with d the spatial dimension [48]. The Brout argument is correct, provided the correlation length is finite, such that the system will eventually self-average. However, at a critical point, the correlation length is infinite, and self-averaging is violated. In that case, the fluctuations decay slower, $k = 1/\nu$, with ν the critical exponent of the correlation length [45,46]. Note that, since fluctuations may never decay faster than self-averaging, an interesting inequality $\nu > 2/d$ is implied, which we immediately recognize to be the Harris criterion [20,49,50].

For this analysis, it is important to use a sufficiently large number of quenched disorder samples. In comparison to lattice models of the RIM universality class, our *off-lattice* fluid simulations are at a disadvantage here, since the number of samples that could be simulated was restricted to $M = 100$. In Fig. 5, we show typical "running averages" of $[z_L]$ and σ_L

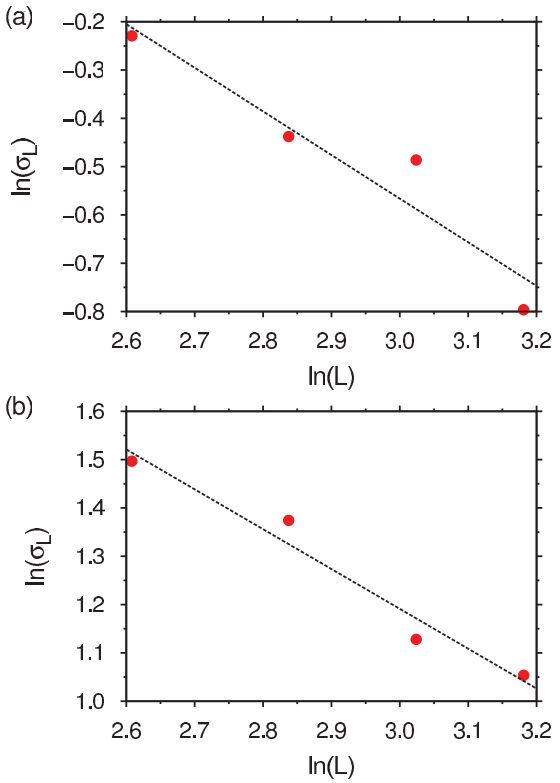

FIG. 6. (Color online) Decay of the fluctuation $\ln \sigma_L$ in the pseudotransition points (defined via the maximum of the susceptibility) as a function of $\ln L$, for porous medium densities $\rho_M = 0.1$ (a) and $\rho_M = 0.2$ (b). The data are approximately linear, indicating a power-law decay $\sigma \propto 1/L^k$, with $k \sim 0.9$ obtained by fitting (dashed lines).

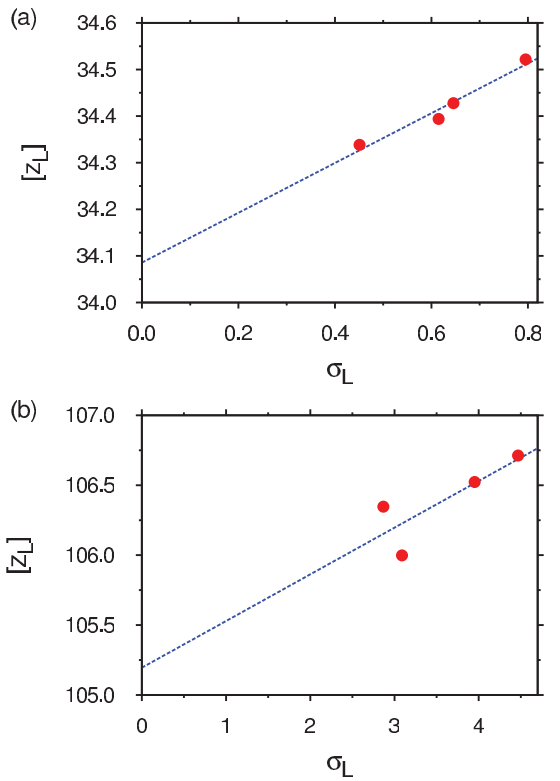

FIG. 7. (Color online) Variation of $[z_L]$ with σ_L, for $\rho_M = 0.1$ (a) and $\rho_M = 0.2$ (b). The dashed lines are linear fits, whose intercepts correspond to z_{cr}.

plotted versus the number of samples M for various system sizes. It appears that the running averages are close to reaching their plateau values, but a larger value of M is clearly desirable. In Fig. 6, we show how σ_L decays with L, for both densities of the porous medium. Note that a double-logarithmic scale is used. The data are compatible with a power-law decay. In addition, the exponent of the decay, $k \sim 0.9$, is smaller than $d/2 = 1.5$, showing that self-averaging is violated, which is indeed expected for RIM universality. However, the actual exponent values are rather far removed from the RIM values (as were our ν estimates of Fig. 4). We believe the most likely explanation is the limited number of porous medium realizations that we could simulate, which suggests that σ_L could not be determined very accurately.

The fact that $\sigma_L \propto 1/L^{1/\nu}$ is also interesting in relation to the average pseudotransition point $[z_L]$, whose shift from its thermodynamic limit value z_{cr} is given by the same form: $z_{cr} - [z_L] \propto 1/L^{1/\nu}$. Consequently, a graph of $[z_L]$ versus σ_L should be linear, with the intercept corresponding to z_{cr}. The result is shown in Fig. 7, for both densities of the porous medium. In both cases, the intercept is within the range of the cumulant intersections of Table I.

D. Distribution of magnetization and susceptibility

Finally, we consider the disorder fluctuation in the actual value of the susceptibility $\chi_{L,i}$ between the quenched disorder samples. To this end, we introduce the normalized squared fluctuation

$$R_\chi = \frac{[\chi_L^2] - [\chi_L]^2}{[\chi_L]^2}, \tag{10}$$

with the disorder average $[\cdot]$ defined as in Eq. (9). Similarly, we also introduce R_m to probe the disorder fluctuation in the "magnetization" $\langle |m| \rangle_{L,i}$ between samples. For each sample of quenched disorder, we thus locate the fugacity $z_{L,i}$ of the susceptibility maximum, then record the corresponding values of $\chi_{L,i}$ and $\langle |m| \rangle_{L,i}$, which are subsequently averaged to yield R_χ and R_m. In this way, we follow the approach of Ref. [43]. Alternatively, one might consider each sample at the same fugacity, say at $[z_L]$, as was done in Ref. [18]. Independent of which method we used, R_m and R_χ increased with the system size, as shown in Fig. 8(a) and Fig. 8(b), respectively. The fact that R_χ and R_m remain finite, as opposed to approaching zero with increasing L, is another signature of self-averaging violation [45,46]. In Fig. 8(c), we plot the ratio R_m/R_χ versus $1/L$. Interestingly, it is very close to the value $1/4$ predicted by renormalization-group theory [18].

Note that, in Fig. 8, only results for $\rho_M = 0.1$ are presented. For $\rho_M = 0.2$, we also observe that R_χ and R_m remain finite, but with significant scatter. This likely reflects a similar issue in these data as in Fig. 7(b), where the data of the largest two systems appear to be systematically off.

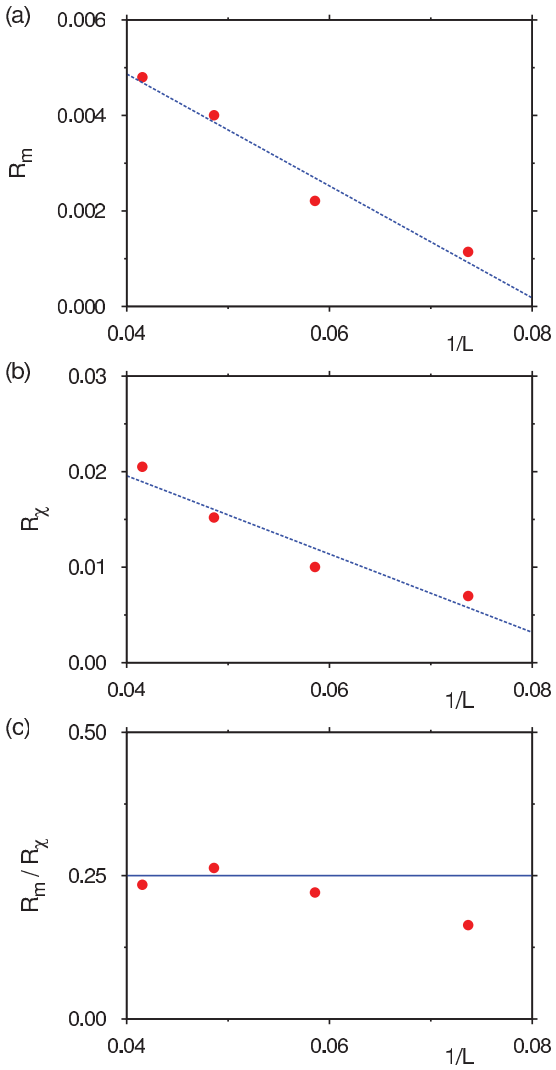

FIG. 8. (Color online) Variation of (a) R_m, and (b) R_χ versus $1/L$, as well as (c) the ratio R_m/R_χ. The lines in (a) and (b) are linear fits meant to guide the eye. The horizontal line in (c) marks the value $1/4$ of renormalization-group theory. All data refer to density of the porous medium $\rho_M = 0.1$.

IV. DISCUSSION

In this work, we have considered the critical behavior of a fluid confined to a random porous medium consisting of neutral walls. Our aim was to confirm the universality class of the corresponding liquid-vapor transition, expected to be the one of the random Ising model. While it remains extremely difficult to obtain accurate critical exponents for this *off-lattice* system, evidence of random Ising behavior is revealed by the disorder fluctuations. By monitoring the fluctuations in the pseudotransition temperatures, the magnetization, and the susceptibility between different realizations of the porous medium, clear violations of self-averaging are observed. Within the limitations of our data, these disorder fluctuations scale with the system size as one would expect for the random Ising model. Nevertheless, it is clear that much more computer power would be needed to reach the accuracy levels attainable in lattice spin models [19]. We surmise that for such a high-resolution study the disorder averages should be calculated over several thousands realizations of the quenched disorder, whereas the present study adopted $M = 100$ samples only.

For such a potential future study, it is advisable to restrict $\rho_M \sim 0.1$ or so. This value is large enough to induce random Ising effects, yet small enough to avoid the severe equilibration problems that set in at higher medium densities. Another quantity that would be interesting to monitor is the coexistence diameter [51]. Following the Harris criterion [20], the critical exponent of the specific heat α is negative for the random Ising model, but positive for the bulk Ising model. Such a change in sign might yield a more pronounced numerical signature in simulation data.

ACKNOWLEDGMENTS

R.V. acknowledges financial support by the German research foundation (Emmy Noether Grant No. VI 483). G.P. acknowledges the National Research Foundation (NRF) of South Africa for financial support through Grant No. 80795.

[1] P. Wiltzius, S. B. Dierker, and B. S. Dennis, Phys. Rev. Lett. **62**, 804 (1989).
[2] A. P. Y. Wong and M. H. W. Chan, Phys. Rev. Lett. **65**, 2567 (1990).
[3] A. P. Y. Wong, S. B. Kim, W. I. Goldburg, and M. H. W. Chan, Phys. Rev. Lett. **70**, 954 (1993).
[4] Y. B. Melnichenko, G. D. Wignall, D. R. Cole, and H. Frielinghaus, Phys. Rev. E **69**, 057102 (2004).
[5] J. V. Maher, W. I. Goldburg, D. W. Pohl, and M. Lanz, Phys. Rev. Lett. **53**, 60 (1984).
[6] P. G. De Gennes, J. Phys. Chem. **88**, 6469 (1984).
[7] T. Nattermann, in *Spin Glasses and Random Fields*, edited by A. P. Young (World Scientific, Singapore, 1998), p. 277.
[8] R. L. C. Vink, T. Fischer, and K. Binder, Phys. Rev. E **82**, 051134 (2010).
[9] N. G. Fytas and V. Martín-Mayor, Phys. Rev. Lett. **110**, 227201 (2013).
[10] R. L. C. Vink, K. Binder, and H. Löwen, Phys. Rev. Lett. **97**, 230603 (2006).
[11] R. L. C. Vink, K. Binder, and H. Löwen, J. Phys.: Condens. Matter **20**, 404222 (2008).
[12] T. Fischer and R. L. C. Vink, J. Phys.: Condens. Matter **23**, 234117 (2011).
[13] T. Fischer and R. L. C. Vink, J. Chem. Phys. **134**, 055106 (2011).
[14] E. Kierlik, M. L. Rosinberg, G. Tarjus, and E. Pitard, Mol. Phys. **95**, 341 (1998).
[15] P. G. De Sanctis Lucentini and G. Pellicane, Phys. Rev. Lett. **101**, 246101 (2008).
[16] H. G. Ballesteros, L. A. Fernández, V. Martín-Mayor, A. Muñoz Sudupe, G. Parisi, and J. J. Ruiz-Lorenzo, Phys. Rev. B **58**, 2740 (1998).

[17] M. Hasenbusch, F. P. Toldin, A. Pelissetto, and E. Vicari, J. Stat. Mech.: Theory Exp. (2007) P02016.
[18] P. E. Berche, C. Chatelain, B. Berche, and W. Janke, Eur. Phys. J. B **38**, 463 (2004).
[19] N. G. Fytas and P. E. Theodorakis, Phys. Rev. E **82**, 062101 (2010).
[20] A. B. Harris, J. Phys. C **7**, 1671 (1974).
[21] W. G. Madden and E. D. Glandt, J. Stat. Phys. **51**, 537 (1988).
[22] W. G. Madden, J. Chem. Phys. **96**, 5422 (1992).
[23] J. Given and G. Stell, Physica A (Amsterdam, Neth.) **209**, 495 (1994).
[24] E. Lomba, J. A. Given, G. Stell, J. J. Weis, and D. Levesque, Phys. Rev. E **48**, 233 (1993).
[25] K. S. Page and P. A. Monson, Phys. Rev. E **54**, 6557 (1996).
[26] M. Alvarez, D. Levesque, and J. J. Weis, Phys. Rev. E **60**, 5495 (1999).
[27] Y. Duda, O. Pizio, and S. Sokolowsi, J. Phys. Chem. **108**, 19442 (2004).
[28] E. Pitard, M. L. Rosinberg, G. Stell, and G. Tarjus, Phys. Rev. Lett. **74**, 4361 (1995).
[29] L. Sarkisov and P. A. Monson, Phys. Rev. E **61**, 7231 (2000).
[30] E. Schöll-Paschinger, D. Levesque, J. J. Weis, and G. Kahl, Phys. Rev. E **64**, 011502 (2001).
[31] G. Pellicane, C. Caccamo, D. S. Wilson, and L. L. Lee, Phys. Rev. E **69**, 061202 (2004).
[32] L. Sarkisov and P. R. van Tassel, J. Chem. Phys. **123**, 164706 (2005).
[33] W. Góźdź, J. Chem. Phys. **119**, 3309 (2003).
[34] D. P. Landau and K. Binder, *A Guide to Monte Carlo Simulations in Statistical Physics* (Cambridge University Press, Cambridge, UK, 2000).
[35] N. B. Wilding, Phys. Rev. E **67**, 052503 (2003).
[36] D. Frenkel and B. Smit, *Understanding Molecular Simulation* (Academic Press, San Diego, 2001).
[37] A. M. Ferrenberg and R. H. Swendsen, Phys. Rev. Lett. **61**, 2635 (1988).
[38] K. Binder, Z. Phys. B **43**, 119 (1981).
[39] N. B. Wilding, J. Phys.: Condens. Matter **9**, 585 (1997).
[40] J. Köfinger, N. B. Wilding, and G. Kahl, J. Chem. Phys. **125**, 234503 (2006).
[41] A. Pelisetto and E. Vicari, Phys. Rep. **368**, 549 (2002).
[42] K. Kaski, K. Binder, and J. D. Gunton, Phys. Rev. B **29**, 3996 (1984).
[43] K. Bernardet, F. Pázmándi, and G. G. Batrouni, Phys. Rev. Lett. **84**, 4477 (2000).
[44] S. Wiseman and E. Domany, Phys. Rev. Lett. **81**, 22 (1998).
[45] S. Wiseman and E. Domany, Phys. Rev. E **58**, 2938 (1998).
[46] A. Aharony and A. B. Harris, Phys. Rev. Lett. **77**, 3700 (1996).
[47] C. Monthus and T. Garel, Eur. Phys. J. B **48**, 393 (2005).
[48] R. Brout, Phys. Rev. **115**, 824 (1959).
[49] A. Aharony, A. B. Harris, and S. Wiseman, Phys. Rev. Lett. **81**, 252 (1998).
[50] J. T. Chayes, L. Chayes, D. S. Fisher, and T. Spencer, Phys. Rev. Lett. **57**, 2999 (1986).
[51] R. L. C. Vink, J. Chem. Phys. **124**, 094502 (2006).